Available online at www.sciencedirect.com
ScienceDirect
Trans. Nonferrous Met. Soc. China 33(2023) 1178−1192
Transactions of Nonferrous Metals Society of China
www.tnmsc.cn

# High-temperature oxidation and TGO growth behaviors of laser-modified YAG/YSZ double-ceramic-layer TBC

Guo-sheng AN[1,2], Wen-sheng LI[1,3], Zhi-ping WANG[2], Li FENG[1,2], Bo CHENG[1], Lan ZHOU[4], Zi-yu LI[2], Yi ZHANG[2]

1. State Key Laboratory of Advanced Processing and Recycling of Non-ferrous Metal, Lanzhou University of Technology, Lanzhou 730050, China;
2. School of Materials Science and Engineering, Lanzhou University of Technology, Lanzhou 730050, China;
3. School of Materials Science and Engineering, Shandong University of Science and Technology, Qingdao 266590, China;
4. School of Mechatronics Engineering, Lanzhou University of Technology, Lanzhou 730050, China

Received 5 December 2021; accepted 27 April 2022

**Abstract:** Yttrium−aluminum garnet/yttria-stabilized zirconia (YAG/YSZ) double-ceramic-layer thermal barrier coating (TBC) with NiCoCrAlY bond coating was deposited by atmospheric plasma spraying (APS) on Inconel 738 alloy substrate, and laser modification was carried out on the surface of YAG ceramic coating to improve the high-temperature oxidation resistance of TBC. Then, isothermal oxidation tests were designed to study the high-temperature oxidation and thermally grown oxide (TGO) growth behaviors of the as-sprayed (AS) and the laser modified (LM) YAG/YSZ TBC. Results show that TGO thickness and structure of both AS-TBC and LM-TBC exhibit the similar evolution trend, TGO thickness increases with the increasing of isothermal oxidation time, and TGO structure develops from single $Al_2O_3$ layer to the double-layer structure of upper mixed oxides and lower $Al_2O_3$. Because of the crucial inhibition effect of the laser modification on oxygen permeation, the appearance time of mixed oxides in LM-TBC is postponed, and the total TGO thickness of LM-TBC is reduced at the middle and final oxidation stages. The $Al_2O_3$ layer thickness proportion of total TGO in LM-TBC is always greater than or equal to that in AS-TBC at the same isothermal oxidation time. Compared with the AS-TBC, the parabolic oxidation rate of LM-TBC is decreased by 18.42%. Therefore, YAG/YSZ LM-TBC presents better oxidation resistance and lower TGO growth rate than AS-TBC.

**Key words:** thermal barrier coating; laser modification; double-ceramic-layer; oxygen permeation; thermally grown oxide

## 1 Introduction

Thermal barrier coating (TBC) has been widely used in nickel-base alloy turbine blades as a protective layer to isolate thermal corrosion and high-temperature oxidation [1,2], because of its superior performances on oxidation, corrosion, and heat resistance [3,4]. A typical TBC is normally composed of yttria-stabilized zirconia (YSZ) ceramic coating as thermal barrier layer, MCrAlY (M=Ni and Co) bond coating as the oxidation-resistant layer and superalloy substrate [5,6]. It is hard for the conventional TBC to meet the ever-increasing high-temperature working conditions, since various complex and interactive failures occurred in TBC during temperature load process [7−9]. Especially, thermal growth stress concentration and crack initiation in TGO bulges induced by the rapid growth of thermal grown oxide (TGO) layer, become the crucial factors to cause TBC spallation and failure [10,11]. However,

**Corresponding author:** Wen-sheng LI, Tel: +86-931-2976706, E-mail: liws@lut.edu.cn
DOI: 10.1016/S1003-6326(23)66174-6

as the main product of TBC oxidation, TGO is an inevitable oxides layer formed along the ceramic coating/bond coating interface when TBC works at high-temperature. Therefore, exploring the avenue of inhibiting TGO formation and growth is extremely urgent to TBC service life.

Oxygen plays the most important role in TGO formation and growth, and ionic diffusion and gas permeation are two major mechanisms for oxygen transport from atmosphere to oxidation reaction interface through YSZ coating. The more the oxygen participates in oxidation reaction, the larger the thickness of TGO layer generated [5]. Double-ceramic-layer TBC system greatly reduced ionic diffusion of oxygen by an additional outer ceramic coating over YSZ, because the additional coating, mainly lanthanum zirconate ($La_2Zr_2O_7$, LZO) and yttrium aluminum garnet ($Y_3Al_5O_{12}$, YAG), acts as a good oxygen barrier for their relatively low oxygen diffusivity. However, gas permeation is usually the most harmful factor. FOX and CLYNE [12] indicated that the oxygen flux caused by gas permeation could be 6.6 times higher than that of ionic diffusion at 1400 K. Although atmospheric plasma spraying (APS) is one of the best ceramic coating deposition technologies for its higher efficiency and lower cost [13,14], serious gas permeation of oxygen would occur in APS TBC. Lamellar structure, which is inevitably produced by the solidification process of APS particles [15], provides sufficient channels for oxygen permeation. On the other hand, some typical APS defects, such as uneven surface with pores and protrusions, can increase the oxidation reaction contact areas between TBC and oxygen, further accelerating the high-temperature oxidation reaction.

More recently, laser technology has attracted considerable attention for fabricating high-precision and high-quality microstructures on a variety of materials [16]. For example, femtosecond laser has been used for generating polytetrafluoroethylene (PTFE) film with unique coral-like micro/nanostructures and stainless steel mesh with large-area periodic nanoripple structures, for obtaining the function of robust self-cleaning passive cooling and oil−water separation, respectively [17,18]. Likewise, several studies have been focused on design the unique TBC microstructures by laser modification for remedying ceramic coating defects after APS deposition. FREITAS et al [19] prepared a dense YSZ ceramic layer with 40 μm in thickness by laser scanning, the microhardness of laser-modified YSZ was higher than that of the as-sprayed YSZ, and surface defects were also reduced. XU et al [20] indicated that the mass gain per unit area of scanned YSZ by low energy density laser was smaller than that scanned by high energy density laser during the cyclic oxidation. Previous studies were mostly focused on the effect of laser modification on microstructure and cycle oxidation of TBC with single ceramic layer, but investigations on how laser-modified structure affects the TGO growth behaviors of TBC with double ceramic layer were rare.

In the present work, the YAG/YSZ double-ceramic-layer TBC was deposited by APS over the NiCoCrAlY bond coating on the Inconel 738 substrates, then laser surface modification was carried out, and thus the as-sprayed (AS) and the laser-modified (LM) TBC were prepared, as shown in Fig. 1. Moreover, isothermal oxidations of AS-TBC and LM-TBC at 1100 ℃ were conducted

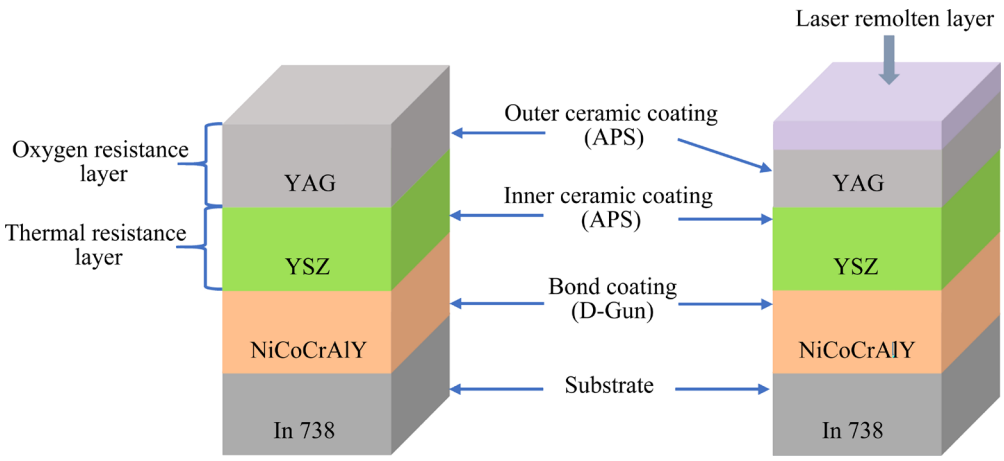


**Fig. 1** YAG/YSZ TBC system: (a) AS-TBC; (b) LM-TBC

to further clarify the effects of inhibiting oxygen permeation on TBC high-temperature oxidation performance and TGO growth behaviors.

## 2 Experimental

Nickel-based superalloy Inconel 738 substrates were cut into circular pieces with size of *d*25.4 mm × 3 mm and then sandblasted. The metallic powder of NiCoCrAlY (Metco, Ni−23Co−17Cr−12Al−0.4Y), ceramic powders of YSZ (Metco, 8 wt.% yttria-stabilized zirconia) and YAG (Baijiaxiang Inc., yttrium aluminum garnet) were employed as feedstock of bond coating, inner ceramic coating and outer ceramic coating, respectively. The morphology and particle size of ceramic powders are shown in Fig. 2. The bond coatings were deposited by the detonation spraying facility (АДМ–4Д, Russia), and then vacuum heat treatment at 1050 ℃ for 2 h were performed in the tube furnace (GSL-1500X-50, China) in order to get a thin $Al_2O_3$ layer as well as increase the adhesion [21]. The ceramic coatings were prepared by the APS facility (GP-80, China), and the YAG surface of AS-TBC was scanning remelted by the fiber laser (IPG YLS-4000) to obtain LM-TBC. The APS and laser scanning parameters are listed in Table 1 and Table 2, respectively.

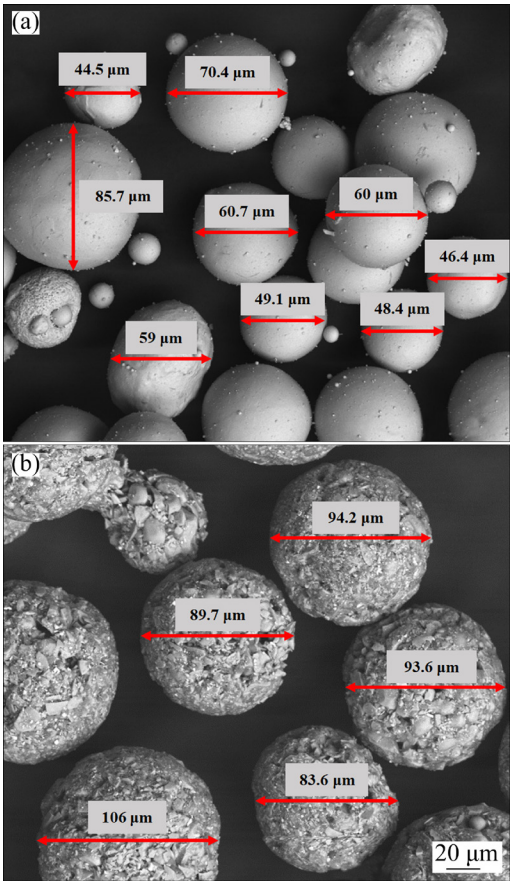


**Fig. 2** Morphologies and particle size distributions of ceramic powders: (a) YSZ; (b) YAG

**Table 1** Parameters of atmospheric plasma spraying [5]

| Coating | Arc current/ A | Arc voltage/ V | Argon flow rate/ (L·min$^{-1}$) | Hydrogen flow rate/ (L·min$^{-1}$) | Spray distance/ mm |
|---|---|---|---|---|---|
| YSZ | 650 | 60 | 60 | 5.5 | 80 |
| YAG | 650 | 55 | 50 | 6.5 | 85 |

**Table 2** Parameters of laser scanning

| Power/ W | Scanning speed/ (mm·s$^{-1}$) | Overlap rate/ % | Spot diameter/ mm |
|---|---|---|---|
| 300 | 50 | 50 | 3 |

The isothermal oxidation tests on AS-TBC and LM-TBC specimens were performed in a muffle furnace (KSL-1800X-A1, China) at 1100 ℃ for 25, 50, 100, 150, 200 and 300 h, and the heating and cooling rates were both 10 ℃/min. The oxidation mass gains were calculated by a precision electronic balance (0.1 mg in precision, Mettler Toledo), and three specimens were tested for average value.

Surface and cross-section microstructural characterizations of AS-TBC and LM-TBC were evaluated by a scanning electron microscope (SEM, Quanta FEG 450) with energy-dispersive X-ray spectroscopy (EDS). Surface roughness was observed by laser scanning confocal microscope (LSCM, Zeiss LSM 800). Porosity and TGO average thickness were calculated by Image-Pro Plus 6.0.

## 3 Results

### 3.1 Microstructural characterization

Figure 3 shows the surface micrographs of AS-TBC and LM-TBC. As shown in Fig. 3(a), AS-TBC presents an uneven surface with pores and protrusions as typical defects of APS, which are caused by insufficient overlapping among the adjacent molten droplets during the flattening process of spraying particles [22]. Although such uneven surface is positive on releasing thermal stress and decreasing thermal conductivity [23], higher roughness enlarges the oxidation reaction

contact areas between as-sprayed layer and external oxygen, further increasing the rates of high-temperature oxidation reaction [24]. After laser scanning, as shown in Fig. 3(b), LM-TBC presents smooth surface with micropores, network cracks as well as hexagonal grains with different sizes, which are caused by insufficient gas escaping time, shrinkage and relaxation of residual stress, and diffuse reflection to the beam after laser irradiation, respectively [25−28]. Note that LM-TBC can achieve obvious lower surface roughness, which is positive to reduce oxidation reaction contact areas between laser remolten layer and external oxygen, and further decreases the rates of high-temperature oxidation reaction.

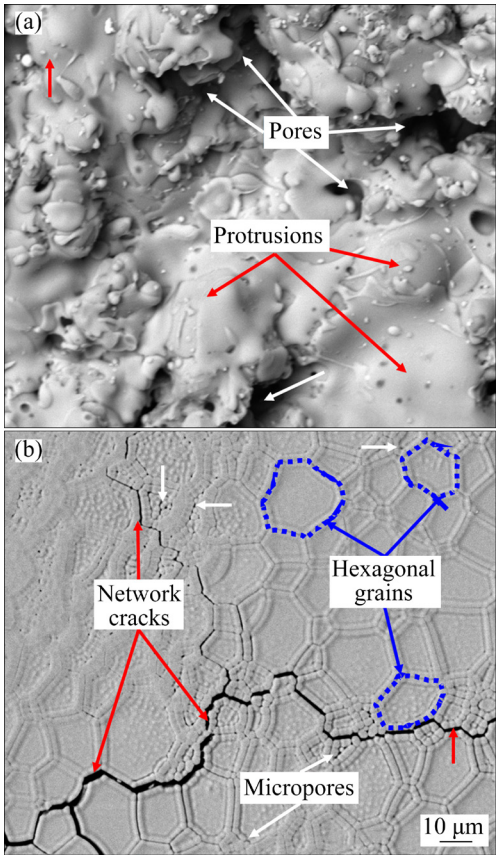


**Fig. 3** Surface morphologies of TBCs: (a) AS-TBC; (b) LM-TBC

Figure 4 shows the cross-sectional micrographs of AS-TBC and LM-TBC. As Fig. 4(a) shows, AS-TBC is composed of outer ceramic coating (YAG), inner ceramic coating (YSZ), and bond coating (NiCoCrAlY), with the thicknesses of (160±20), (160±20), and (110±20) μm, respectively. The YAG coating of AS-TBC has higher porosity (9.43%) and obvious lamellar structure, as shown in Fig. 4(b). As well known, such a microstructure is in favor of oxygen permeation and negative to high-temperature oxidation resistance of TBC. LM-TBC has the same coating composition and corresponding thickness to AS-TBC, except that the outer ceramic coating (YAG) is composed of as-sprayed zone and laser remolten zone, as shown in Fig. 4(c). With the help of remolten compact zone in LM-TBC, porosity of total YAG coating of LM-TBC is decreased to 2.85%. Simultaneously, obvious columnar structure and a few vertical microcracks with the width of 1−2 μm can be observed in laser remolten zone, which are attributed to directional solidification along the heat flow direction and tension stress concentration towards central area, respectively, as shown in Fig. 4(d) [22].

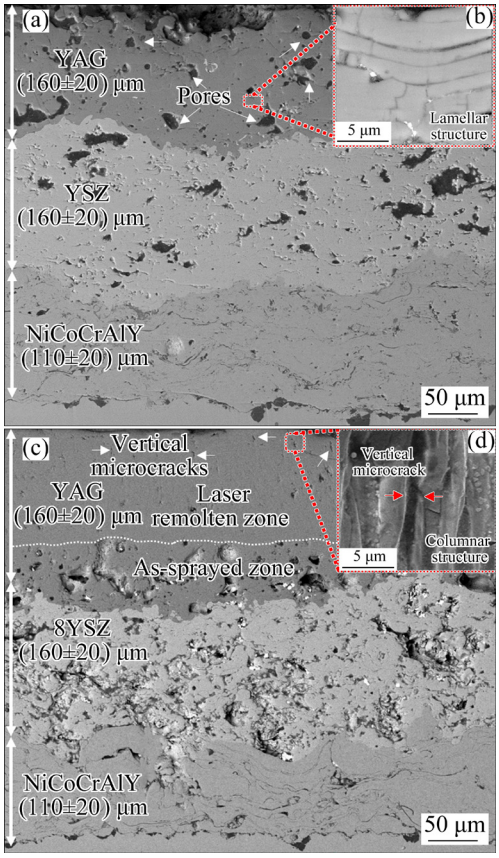


**Fig. 4** Cross-sectional morphologies of TBCs: (a) AS-TBC; (b) Lamellar structure in AS-TBC; (c) LM-TBC; (d) Vertical microcrack and columnar structure in LM-TBC

### 3.2 TGO formation and growth

Figure 5 shows the amplified TGO micrographs of AS-TBC and LM-TBC isothermally oxidized at 1100 ℃ for different time. After 25 h

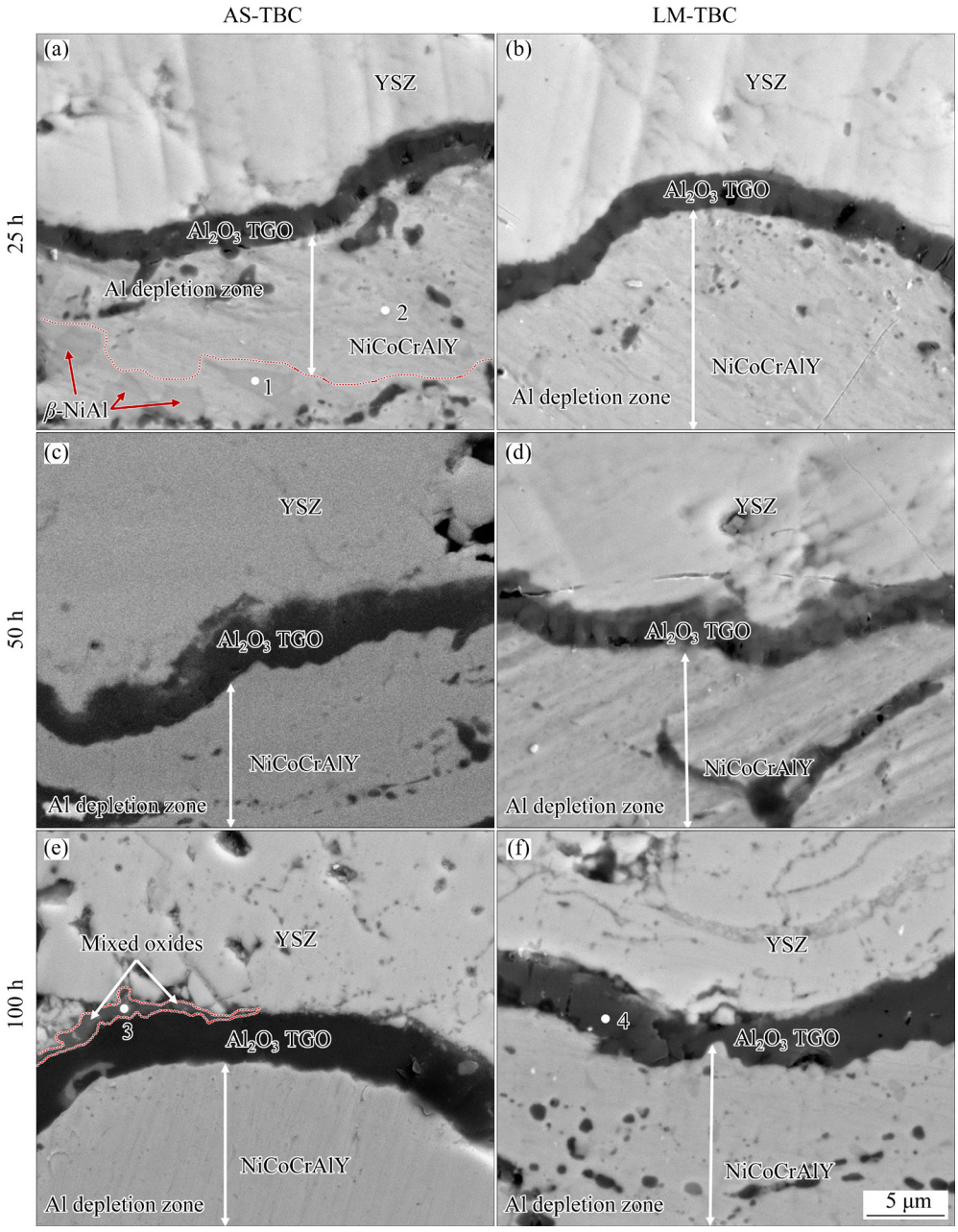


**Fig. 5** Amplified TGO morphologies of TBCs oxidized at 1100 °C for different time

oxidation, a dense and black $Al_2O_3$ TGO layer (~2.38 μm) is formed along the NiCoCrAlY/YSZ interface of AS-TBC, as shown in Fig. 5(a). The EDS results of Points 1 and 2 in Table 3 indicate that the $Al^{3+}$ first diffuses to the interface and reacts with $O^{2-}$ to form the black $Al_2O_3$ layer, and then $\beta$-NiAl (grey patches) is surrounded by the depletion zone of Al in bond coating. And it seems that the less the $Al^{3+}$ participates in the oxidation reaction, the more the $\beta$-NiAl is left in bond coating, and the smaller the $Al_2O_3$ TGO thickness is generated. Hence, the $Al_2O_3$ TGO layer thickness (~2.73 μm) of LM-TBC is larger than that of AS-TBC, since there is almost no $\beta$-NiAl (grey patches) left in bond coating, as shown in Fig. 5(b). This indicates that more serious oxidation occurs in LM-TBC at the initial oxidation stage.

With the isothermal oxidation time is extended to 50 h, the bond coatings of AS-TBC and LM-TBC present totally depletion zone of Al, as shown in Figs. 5(c, d). This phenomenon demonstrates that large amount of $Al^{3+}$ in bond coatings is used for generating $Al_2O_3$, the $Al_2O_3$ TGO thicknesses of AS-TBC and LM-TBC increased to 3.42 and 2.94 μm, respectively, and the TGO thickness increasing percentages are 43.70% and 7.69%

compared with those of TBCs isothermally oxidized for 25 h, respectively. Higher increasing percentages indicate that the TGO growth rate of AS-TBC is higher than that of LM-TBC during the 25−50 h isothermal oxidation period. Till to100 h, the TGO thicknesses of AS-TBC and LM-TBC are 5.50 and 3.70 μm, and the corresponding TGO thickness increasing percentages are 60.82% and 25.85%, respectively. The lower TGO thickness increasing percentage of LM-TBC indicates that laser surface modification effectively decreases the TGO growth rate at the middle oxidation stage. After 100 h, as shown in Fig. 5(e), there is a very small grey region appearing at the YSZ/$Al_2O_3$ TGO interface of AS-TBC, and the EDS result of Point 3 reveals that the grey region is mixed oxides which are rich in Ni, Cr, and Co. Hence, the total AS-TBC TGO consists of mixed oxides layer (~1.12 μm) and $Al_2O_3$ layer (~4.38 μm). The TGO morphology of AS-TBC presents a double-layer structure although the mixed oxides layer is very thin. However, according to the TGO morphology and EDS result of Point 4 in Table 3, the TGO structure of LM-TBC still retains single $Al_2O_3$ layer, as shown in Fig. 5(f).

**Table 3** EDS analysis result of different points in Fig. 5 (at.%)

| Point | Ni | Co | Cr | Al | O |
|---|---|---|---|---|---|
| 1 | 51.6 | 9.3 | 4.6 | 33.1 | 1.4 |
| 2 | 37.8 | 25.1 | 25.3 | 9.8 | 2.0 |
| 3 | 9.4 | 7.5 | 7.5 | 31.8 | 43.8 |
| 4 | 0.2 | 0.3 | 0.1 | 48.0 | 51.5 |

After isothermal oxidization for 150 h, Fig. 6(a) shows that the TGO of AS-TBC exhibits an observable grey and black double-layer structure, and the total TGO thickness is 8.33 μm, which is composed of mixed oxides (grey layer) of 2.62 μm and $Al_2O_3$ (black layer) of 5.71 μm. However, the LM-TBC TGO component is only caused by the $Al^{3+}$ diffusion, without any other metallic element indexed, so its TGO is still a single black $Al_2O_3$ layer with the thickness of 4.62 μm, as shown in Fig. 6(b).

After isothermal oxidization for 200 h, both AS-TBC and LM-TBC present the same double-layer structure: grey mixed oxides on the upper and black $Al_2O_3$ on the lower, but with different thicknesses and compositions, as shown in Figs. 7(a, b). The thickness of mixed oxides and $Al_2O_3$ are 4.38 and 4.77 μm in AS-TBC, but 1.80 and 6.69 μm in LM-TBC. The thickness of total TGO and mixed oxides in AS-TBC is larger than that in LM-TBC, and $Al_2O_3$ layer thickness proportion of total TGO in AS-TBC is obviously lower than that in LM-TBC. The higher the $Al_2O_3$ proportion of TGO is, the stronger the ability to insulate metallic cation diffusion is, so LM-TBC possesses better protection effect on bond coating than AS-TBC in the period of isothermal oxidation.

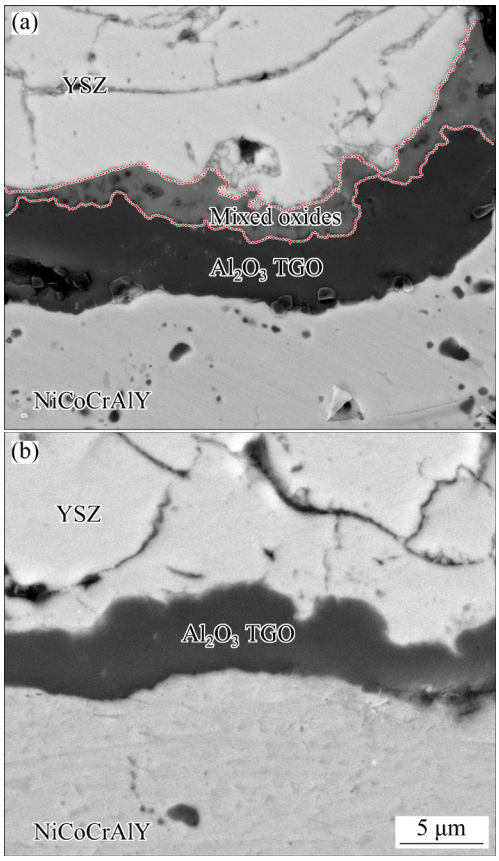


**Fig. 6** Amplified TGO morphologies of TBCs oxidized at 1100 °C for 150 h: (a) AS-TBC; (b) LM-TBC

In order to further investigate the elements distribution in AS-TBC TGO bulge site, EDS line-scan profile was performed along the green line in Fig. 7(a). The results show that across the total TGO, from the top ceramic coating to the bottom bond coating, there are four regions, i.e., the ceramic coating (YSZ), the mixed oxides, the $Al_2O_3$, and the bond coating (NiCoCrAlY). In the region of 0−4.35 μm along *x*-axis, where the YSZ coating locates, there is a lot of Zr element, a small amount of Y and O elements. In the region of 4.35−9.40 μm

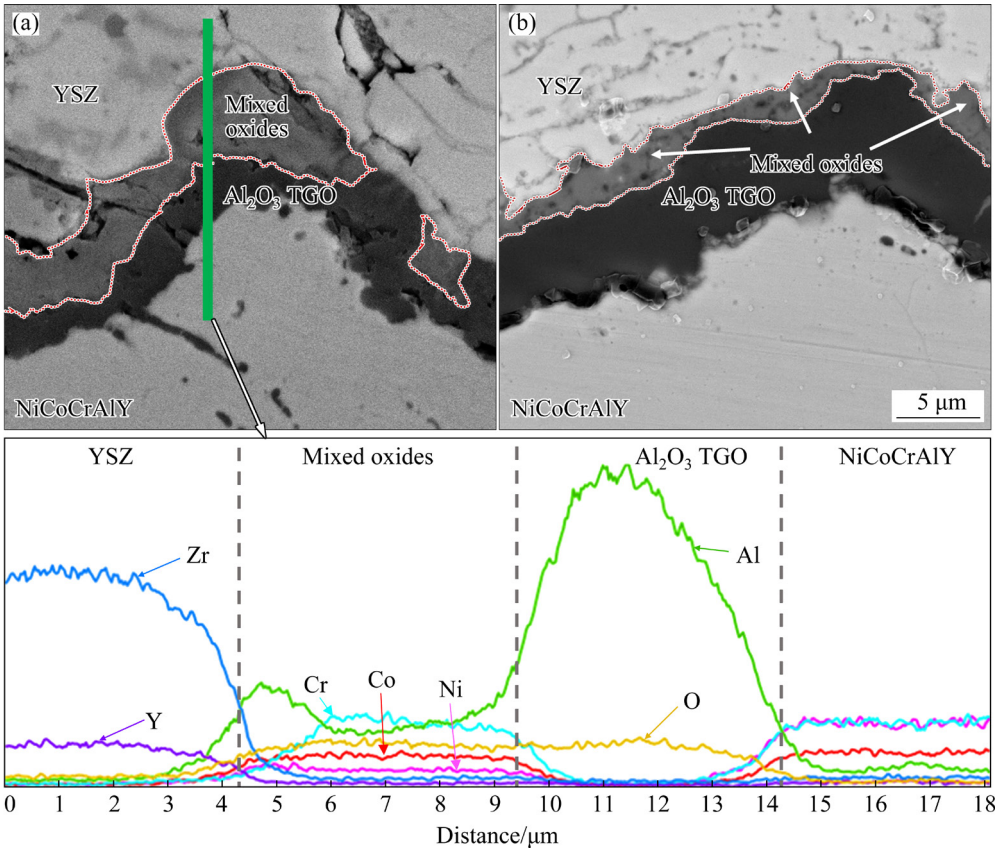


**Fig. 7** Amplified TGO morphologies of TBCs oxidized at 1100 °C for 200 h: (a) AS-TBC; (b) LM-TBC

along *x*-axis where the mixed oxides locate, Ni, Co and Cr elements present a hump shape. In the region of 9.40−14.25 μm along *x*-axis where the $Al_2O_3$ TGO locates, Al and O amounts reach the maximum and the amounts of other elements are almost close to zero. In region of 14.25−18.10 μm along *x*-axis, the bond coating mainly consists of Ni, Co, and Cr, and a small amount of Al and Y.

When the isothermal oxidation time is extended to 300 h, as shown in Figs. 8(a, b), the total TGO thicknesses of AS-TBC and LM-TBC are 13.68 and 11.51 μm, respectively. There are intuitively more sharp interfacial fluctuations and lager thickness of mixed oxides in AS-TBC than those in LM-TBC. It should be noted that the inner crack with length of 17.01 μm is created in the mixed oxides bulge zone of AS-TBC. The TGO inner crack would accelerate the propagation of horizontal cracks, leading to more serious oxidation in AS-TBC, and ultimately induce coating spallation [28]. As shown in Figs. 8(c, d), EDS results exhibit that the grey region with porous microstructure on the upper part is mixed oxide rich in Ni, Cr, and Co (circled by a red dotted line), and the black region with higher compactness on the lower part is $Al_2O_3$.

### 3.3 Evolution of TGO and YAG surface

A dense and continuous $Al_2O_3$ layer plays a positive role on inhibiting the excessive growth of TGO. Due to its slower growth rate, better adhesion [29], and superior oxidation protection on TBC at high temperature, $Al_2O_3$ layer is the most desirable oxide scale in TGO [30]. In order to further clarify the $Al_2O_3$ layer growth processes of AS-TBC and LM-TBC in Figs. 5−8, Fig. 9 is drawn to evaluate the TGO composition and thickness in the isothermal oxidation process.

As shown in Fig. 9, the $Al_2O_3$ layer thickness in LM-TBC (2.73 μm) is larger than that in AS-TBC (2.38 μm) at the initial oxidation stage (25 h) of isothermal oxidation. With extending the isothermal oxidation time (50−300 h), although both the thickness of total TGO and the thickness of mixed oxides in AS-TBC and LM-TBC are increased, the thickness in LM-TBC is always smaller than that in AS-TBC. Additionally, the mixed oxides appear in AS-TBC after 100 h

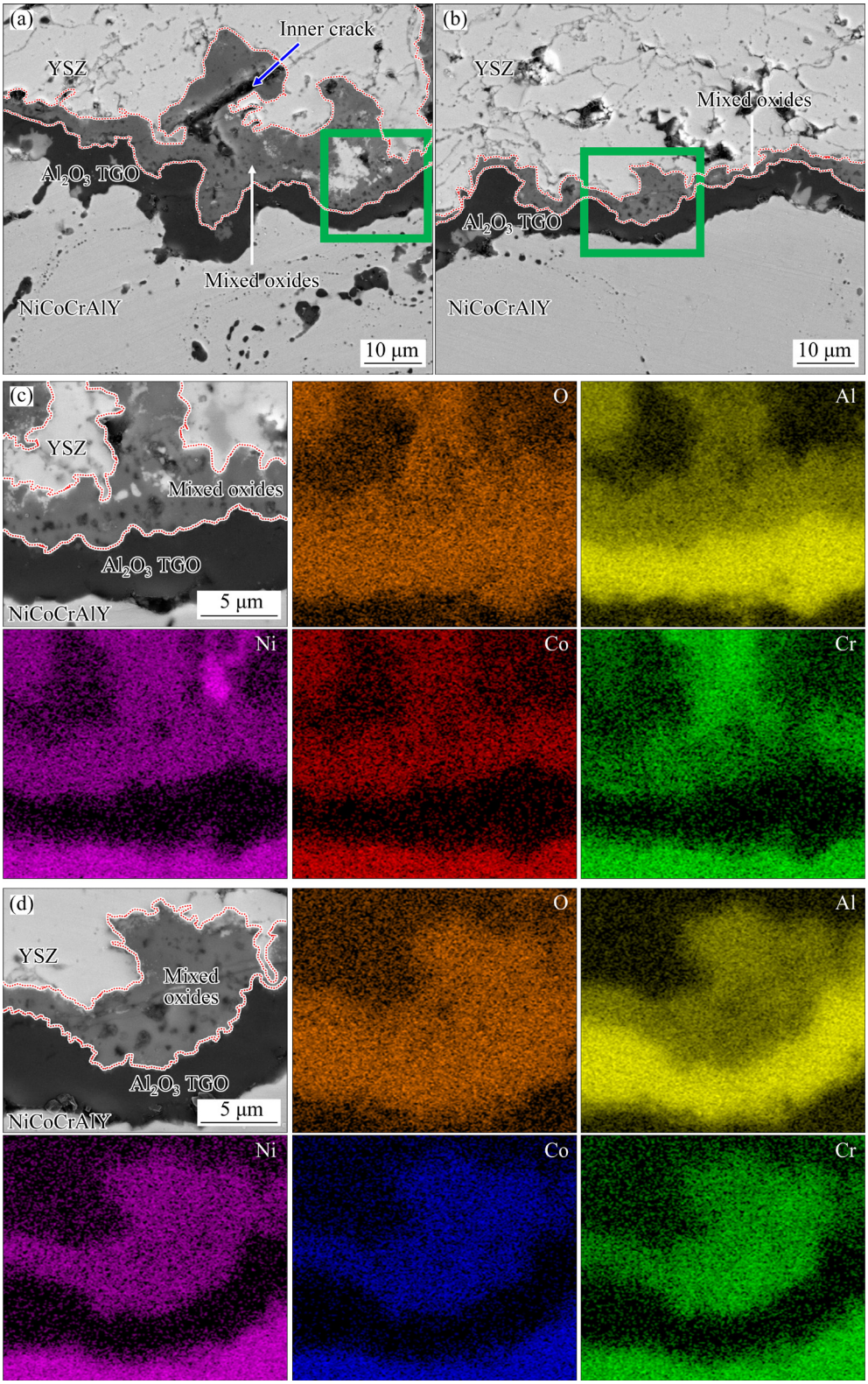


**Fig. 8** TGO morphologies (a, b) and elements distributions (c, d) of TBCs oxidized at 1100 °C for 300 h: (a, c) AS-TBC; (b, d) LM-TBC

oxidation, but it is obviously postponed to 200 h in LM-TBC. This indicates that the oxidation reaction rate of LM-TBC is significantly decreased compared with that of AS-TBC at the middle and final oxidation stages.

As shown in Fig. 9, the $Al_2O_3$ layer thickness proportion of total TGO in AS-TBC is 100% till being oxidized for 50 h, and then reduces to 79.64%,

68.56%, 52.13% and 46.42%, after being oxidized for 100, 150, 200 and 300 h, respectively. However, the $Al_2O_3$ layer thickness proportion of total TGO in LM-TBC is 100% till being oxidized for 150 h, and then reduces to 78.80% and 62.12% after being oxidized for 200 and 300 h, respectively. It is suggested that the $Al_2O_3$ layer thickness proportion of total TGO in LM-TBC is always greater than or equal to that in AS-TBC in the entire isothermal oxidation process. This phenomenon is beneficial to decreasing TGO growth rate in LM-TBC, since the bond coating metallic elements has the lowest diffusion coefficient in $Al_2O_3$ [22].

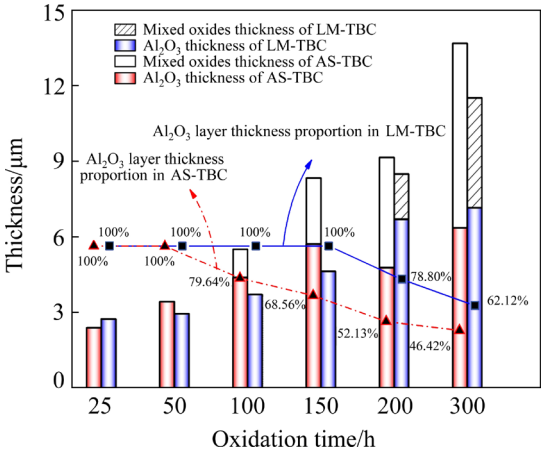


**Fig. 9** TGO composition and thickness in AS-TBC and LM-TBC

In order to evaluate the relationship between ceramic coating surface morphology and TGO growth rate, the surface morphology and roughness of both AS-TBC and LM-TBC after 1100 °C oxidation for 300 h were analyzed. Compared with the original surface morphology of AS-TBC shown in Fig. 3(a), more cracks with different sizes appear on the YAG surface of ceramic coating after long-time oxidation, as shown in Fig. 10(a). Moreover, these cracks provide more and more permeating channels of oxygen, leading to the continuously accelerated oxidation reaction rate. As a result, the YAG surface roughness of AS-TBC is significantly increased. On the contrary, nearly all the original network cracks of LM-TBC are healed during thermal fatigue, as shown in Fig. 10(b). Compared with the surface morphology before oxidation shown in Fig. 3(b), the YAG surface without open cracks obviously reduces oxygen permeating channels in ceramic coating, and further postpones the TGO growth in LM-TBC. On the other hand, with the help of crack healing, the damage induced by thermal stress is effectively decreased in LM-TBC, so the oxidation reaction degree of LM-TBC is much lower than that of AS-TBC. By contrast, the YAG surface of LM-TBC only undergoes a slight damage and its surface roughness has little variation after oxidation. The YAG surface roughness variation trends of AS-TBC and LM-TBC are shown in Fig. 11.

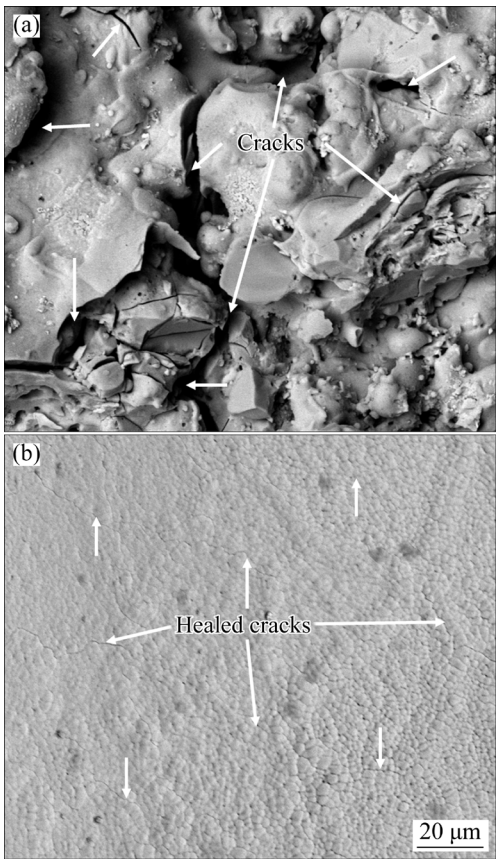


**Fig. 10** Surface morphologies of TBCs after oxidation at 1100 °C for 300 h: (a) AS-TBC; (b) LM-TBC

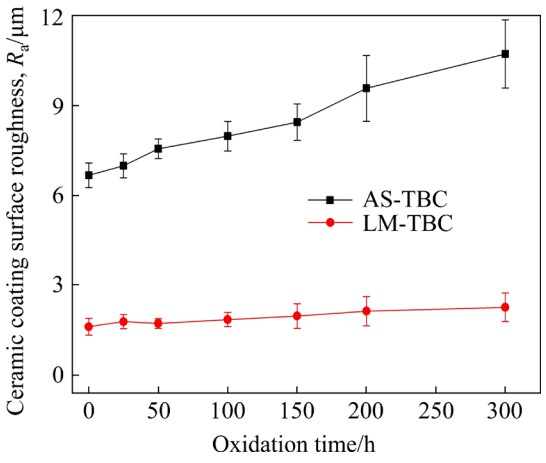


**Fig. 11** YAG surface roughness of AS-TBC and LM-TBC after different isothermal oxidation time

## 4 Discussion

### 4.1 TGO oxidation kinetics

The oxidation kinetics curves of TBCs indicated that the oxidation kinetics of AS-TBC and LM-TBC exhibited a parabolic law [31], as shown in Fig. 12(a). The oxidation mass gain of LM-TBC was greater than that of AS-TBC only at the initial oxidation stage, but always lower at the middle and final oxidation stages due to its better high-temperature oxidation resistance. Figure 12(b) showed that the parabolic constant $K_p$ values of AS-TBC and LM-TBC by fitting the kinetic curves were 4.18 and 3.41 $mg^2 \cdot cm^{-4} \cdot h^{-1}$, respectively. This result illustrated that the parabolic oxidation rate of LM-TBC was decreased by 18.42% compared with that of AS-TBC.

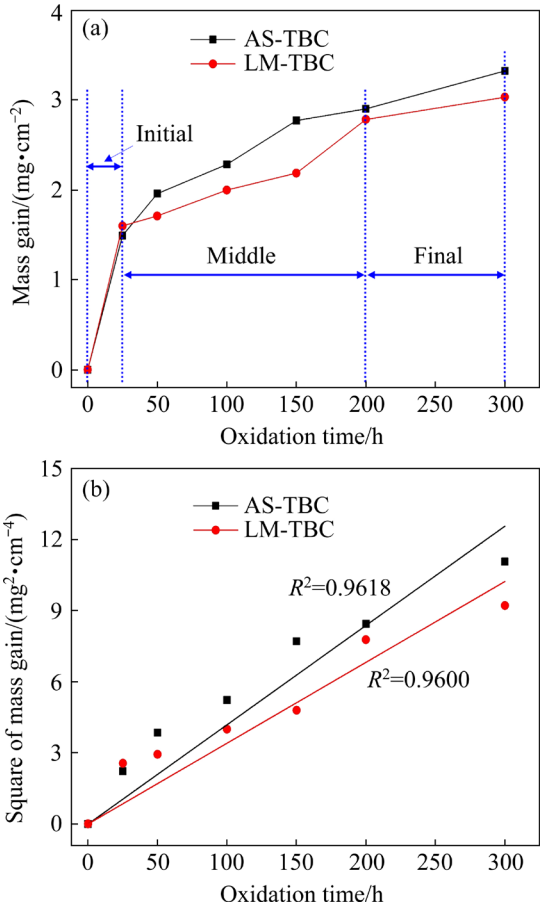


**Fig. 12** Isothermal oxidation kinetics curves at 1100 °C of TBCs: (a) Mass gain; (b) Parabolic constant $K_p$ fitting

### 4.2 High-temperature oxidation resistance mechanisms

LM-TBC presented lower oxidation reaction rate than AS-TBC, for its smaller total TGO thickness, higher $Al_2O_3$ layer thickness proportion of total TGO, less oxidation mass gain, and lower parabolic constants $K_p$ in the entire isothermal oxidation process. The lower oxidation reaction rate was resulted from less oxygen participated in the oxidation reaction, namely less oxygen arriving at ceramic coating/bond coating interface of TBC.

A schematic illustration of oxygen permeation and TGO growth mechanism of AS-TBC and LM-TBC at different isothermal oxidation stages is shown in Fig. 13. In the process of isothermal oxidation, external oxygen diffused through ceramic coating and arrived at oxidation reaction interface by gas permeation and ionic diffusion. The diffusion of oxygen ions in AS-TBC should be same as that in LM-TBC, since the two ceramic coatings had the same materials and thickness, only with different microstructures. Therefore, the different gas permeation resulted from different microstructures is a major principal concern.

As Fig. 13(a) showed, before isothermal oxidation, AS-TBC and LM-TBC had the same constitution and thickness of each coating, located on left and right parts of the blue arrow, respectively. The amplified microstructure characteristics of YAG coating with the same thickness in AS-TBC as-sprayed zone and LM-TBC laser remolten zone were highlighted by green dotted rectangular frames (Figs. 13(a-1) and (a-2), respectively). Remarkable characteristics of AS-TBC were uneven surface with many defects and lamellar structure, as shown in Fig. 13(a-1), and LM-TBC had lower surface roughness but with network cracks, vertical microcracks and columnar structure, as shown in Fig. 13(a-2).

As Fig. 13(b) showed, at the initial isothermal oxidation stage less than 25 h, there were sufficient $O^{2-}$ diffusing into AS-TBC YAG coating through the APS defects and lamellar structure of AS-TBC (Fig. 13(b-1)), but intuitively more $O^{2-}$ diffused into LM-TBC YAG coating, since network cracks and vertical microcracks of laser remolten zone provided more open permeating channels of oxygen (Fig. 13(b-2)). Then, different amounts of $O^{2-}$ in both TBCs continuously diffused into the untreated YAG and YSZ coatings, but finally less $O^{2-}$ could arrive at the interface of ceramic coating/bond coating, as shown in Figs. 13(b-3, b-4). This was mainly attributed to the fact that most of oxygen ionic diffusion was hindered by YAG coating due to

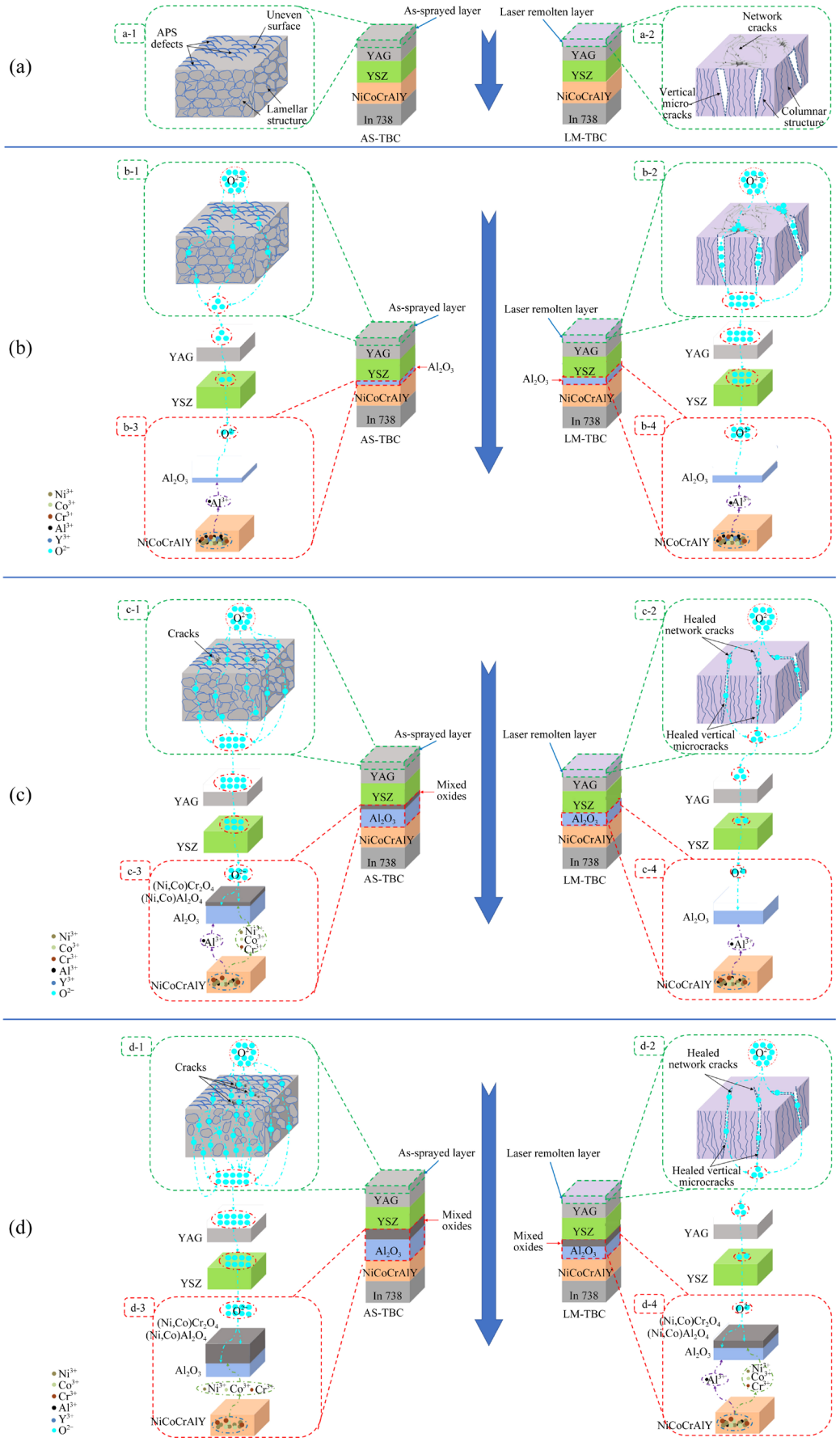


**Fig. 13** Schematic illustration of oxygen permeation and TGO growth mechanism of AS-TBC and LM-TBC at different isothermal oxidation stages: (a) Before oxidation; (b) Initial oxidation; (c) Middle oxidation; (d) Final oxidation

its very low oxygen diffusivity ($10^{-20}$ $m^2/s$) [32]. After that, although the same oxidation reactions occurred in AS-TBC and LM-TBC: Al preferentially participated in oxidation to form $Al_2O_3$ which has the lowest Gibbs free energy in TGO [33,34], more $O^{2-}$ arrived at the oxidation reaction interface of LM-TBC to form a larger thickness of $Al_2O_3$ in LM-TBC than that in AS-TBC.

As Fig. 13(c) showed, at the middle isothermal oxidation stage from 50 to 150 h, AS-TBC presented more uneven surface with obvious cracks and looser lamellar structure (Fig. 13(c-1)), and LM-TBC presented denser surface and cross-section morphology due to the network cracks and vertical microcracks began to heal (Fig. 13(c-2)). The total thermal stress, which was originated from isotropic thermal expansion misfit and anisotropic TGO growth, was partly released by non-uniformed strain of lamellar structure in AS-TBC and cracks healing of laser remolten zone in LM-TBC, respectively [35,36]. Hence, the different morphology evolutions mentioned above in AS-TBC and LM-TBC could be observed. Moreover, this denser surface and cross-section structure of LM-TBC further limited oxygen transportation by eliminating open permeating channels of oxygen [37], and contributed to achieve better oxidation resistance of LM-TBC in this stage.

According to second law of thermodynamics and Gibbs free energy of oxides spontaneous formation [38], the more the $O^{2-}$ arrived at the oxidation reaction interface, the more the $Al^{3+}$ diffused outward from bond coating to form $Al_2O_3$, the less the $Al^{3+}$ left in bond coating, and thus the larger the thickness of $Al_2O_3$ TGO achieved. When the $Al^{3+}$ content in bond coating was below a level of concentration and under sufficient partial pressure of oxygen, other metallic elements would spontaneously diffuse outward and react with $O^{2-}$ to form NiO, CoO, $Cr_2O_3$, and spinels [39], such as $(Ni,Co)Al_2O_4$ and $(Ni,Co)Cr_2O_4$. Therefore, larger TGO thickness with double-layer structure could be observed in AS-TBC, as shown in Fig. 13(c-3). However, compared with AS-TBC, due to the fact that less $Al^{3+}$ was consumed in LM-TBC, the TGO of LM-TBC still retained single $Al_2O_3$ layer, as shown in Fig. 13(c-4).

As Fig. 13(d) showed, at the final isothermal oxidation stage from 200 to 300 h, AS-TBC presented larger size cracks and looser structure with the isothermal oxidation time extending. These damaged surface and cross-section greatly helped large amount of oxygen to easily permeate through ceramic coating, leading to more serious damages to AS-TBC (Fig. 13(d-1)). Conversely, the amount of $O^{2-}$, which could arrive at the oxidation reaction interface of LM-TBC, was greatly reduced than that of AS-TBC at this oxidation stage (Fig. 13(d-2)). This was attributed to the fact that the dense remolten zone of LM-TBC closed most permeating channels of oxygen by continuous healing the network cracks and vertical microcracks. As a result, the degree of oxidation reaction and damage occurring in LM-TBC were rather limited at the final oxidation stage, even though the total amount of $O^{2-}$ diffusing through ceramic coating increased than before.

The excessive consumption of $Al^{3+}$ led to $Ni^{2+}$, $Cr^{3+}$ and $Co^{2+}$ in bond coating rapid diffusing through $Al_2O_3$ TGO to form mixed oxides, and thus the double-layer TGO structure thickness, especially mixed oxides thickness of AS-TBC was greatly increased (Fig. 13(d-3)). And correspondingly, less consumption of $Al^{3+}$ contributed to mixed oxides thickness and appearance time in LM-TBC smaller and later than those in AS-TBC (Fig. 13(d-4)). Therefore, LM-TBC obviously decreased oxidation reaction rate and exhibited superior high-temperature oxidation resistance than AS-TBC.

## 5 Conclusions

(1) Laser modification had crucial inhibition effect on oxygen permeation, the total TGO growth rate of LM-TBC is obviously slower than that of AS-TBC during the isothermal oxidation at 1100 ℃, and parabolic oxidation rate of LM-TBC ($3.41\ mg^2\cdot cm^{-4}\cdot h^{-1}$) is decreased by 18.42% compared with that of AS-TBC ($4.18\ mg^2\cdot cm^{-4}\cdot h^{-1}$).

(2) With the isothermal oxidation time extending, the TGO structure of both TBCs develops from single $Al_2O_3$ layer to double-layer of upper mixed oxides and lower $Al_2O_3$. But the adverse mixed oxides appearance time and thickness of AS-TBC are earlier and larger than those of LM-TBC, and the $Al_2O_3$ layer thickness proportion of total TGO in LM-TBC is always

larger than or equal to that in AS-TBC.

(3) Modifying the YAG coating by laser scanning with a remolten layer microstructure is a promising method to reduce permeating channels of oxygen, inhibit TGO growth and can further improve high-temperature oxidation resistance of YAG/YSZ double-ceramic-layer TBC.

## Acknowledgments

This work was supported by Major Special Projects of Gansu Province, China (No. 21ZD4WA017), University Industry Transformation Promotion Project of Gansu Province, China (No. 2020C-11), the Program of "Science and Technology International Cooperation Demonstrative Base of Metal Surface Engineering along the Silk Road", China (No. 2017D01003), and the National Natural Science Foundation of China (No. 51901093).

## References

[1] ZHANG Xun, COCKS A C F, OKAJIMA Y, TAKENO K, TORIGOE T. An image-based model for the sintering of air plasma sprayed thermal barrier coatings [J]. Acta Materialia, 2021, 206: 116649.

[2] ZHAO Su-mei, YAN Peng-tao, GAO Jiao-jiao, ZHOU Ling, ZHANG Zan, LI Yin-feng, QIAO Jian-sheng, LIU Bin. Characterization and hot corrosion behavior of the $La_2(Zr_{0.7}Ce_{0.3})_2O_7$/8YSZ: Eu double ceramic layer coating prepared by atmospheric plasma spraying [J]. Surfaces and Interfaces, 2020, 21: 100777.

[3] ZHANG Xiao-feng, NIU Shao-peng, DENG Zi-qian, LIU Min, LI Hong, DENG Chun-ming, DENG Chang-guang, ZHOU Ke-song. Preparation of $Al_2O_3$ nanowires on 7YSZ thermal barrier coatings against CMAS corrosion [J]. Transactions of Nonferrous Metals Society of China, 2019, 29: 2362−2370.

[4] LUO Li-rong, SHAN Xiao, ZOH Zhong-hua, ZHAO Chun-shan, WANG Xin, ZHANG Ai-ping, ZHAO Xiao-Feng, GUO Fan-wei, XIAO Ping. A high performance NiCoCrAlY bond coat manufactured using laser powder deposition [J]. Corrosion Science, 2017, 126: 356−365.

[5] AN Guo-sheng, LI Wen-sheng, FENG Li, CHENG Bo, WANG Zhi-ping, LI Zi-yu, ZHANG Yi. Isothermal oxidation and TGO growth behaviors of YAG/YSZ double-ceramic-layer thermal barrier coatings [J]. Ceramics International, 2021, 47: 24320−24330.

[6] VOURDAS N, MARATHONITI E, PANDIS P K, ARGIRUSIS Chr, SOURKOUNI G, LEGROS C, MIRZA S, STATHOPOULOS V N. Evaluation of $LaAlO_3$ as top coat material for thermal barrier coatings [J]. Transactions of Nonferrous Metals Society of China, 2018, 28: 1582−1592.

[7] ZAKERI A, BAHMANI E, AGHDAM A S R, SAEEDI B, BAI M. A study on the effect of nano-$CeO_2$ dispersion on the characteristics of thermally-grown oxide (TGO) formed on NiCoCrAlY powders and coatings during isothermal oxidation [J]. Journal of Alloys and Compounds, 2020, 835: 155319.

[8] LIU Qiao-mu, HUANG Shun-zhou, HE Ai-jie. Composite ceramics thermal barrier coatings of yttria stabilized zirconia for aero-engines [J]. Journal of Materials Science & Technology, 2019, 35: 2814−2823.

[9] GONG Shan-shan, CHEN Ming, HUANG Xun-peng, ZHANG Fan. CMAS resistance characteristics of $RE_{50}Ta_xZr_{50-x}O_{175+0.5x}$ thermal barrier oxides in $RE_2Zr_2O_7$-$RETaO_4$ systems [J]. Transactions of Nonferrous Metals Society of China, https://kns.cnki.net/kcms/detail/43.1239.TG.20220125.0930.012.html.

[10] MENG Guo-hui, LIU Hong, XU Peng-yun, LI Guang-rong, XU Tong, YANG Guan-jun, LI Chang-jiu. Superior oxidation resistant MCrAlY bond coats prepared by controlled atmosphere heat treatment [J]. Corrosion Science, 2020, 170: 108653.

[11] WANG Le, DI Yue-lan, LIU Ying, WANG Hai-dou, YOU Hao-xing, LIU Tao. Effect of TGO on the tensile failure behavior of thermal barrier coatings [J]. Frontiers of Mechanical Engineering, 2019, 14: 452−460.

[12] FOX A C, CLYNE T W. Oxygen transport by gas permeation through the zirconia layer in plasma sprayed thermal barrier coatings [J]. Surface and Coatings Technology, 2004, 184: 311−321.

[13] JIA Sheng-kai, ZOU Yong, XU Ji-yuan, WANG Jing, YU Lei. Effect of $TiO_2$ content on properties of $Al_2O_3$ thermal barrier coatings by plasma spraying [J]. Transactions of Nonferrous Metals Society of China, 2015, 25: 175−183.

[14] JIANG Peng, YANG Liu-yu, SUN Yong-le, LI Ding-jun, WANG Tie-jun. Nondestructive measurements of residual stress in air plasma-sprayed thermal barrier coatings [J]. Journal of the American Ceramic Society, 2021, 104: 1455−1464.

[15] GILDERSLEEVE E J, VISWANATHAN V, LANCE M J, HAYNES J A, PINT B A, SAMPATH S. Role of bond coat processing methods on the durability of plasma sprayed thermal barrier systems [J]. Surface and Coatings Technology, 2019, 375: 782−792.

[16] YIN Kai, DU Hai-feng, LUO Zhi, DONG Xin-ran, DUAN Ji-an. Multifunctional micro/nano-patterned PTFE near-superamphiphobic surfaces achieved by a femtosecond laser [J]. Surface and Coatings Technology, 2018, 345: 53−60.

[17] WU Jun-rui, HE Jun, YIN Kai, ZHU Zhuo, XIAO Si, WU Zhi-peng, DUAN Ji-an. Robust hierarchical porous PTFE film fabricated via femtosecond laser for self-cleaning passive cooling [J]. Nano Letters, 2021, 21: 4209−4216.

[18] YIN Kai, CHU Dong-kai, DONG Xin-ran, WANG Cong, DUAN Ji-an, HE Jun. Femtosecond laser induced robust periodic nanoripple structured mesh for highly efficient oil−water separation [J]. Nanoscale, 2017, 9: 14229−14235.

[19] FREITAS F E, BRIGUENTE F P, REIS A G, VASCONCELOS G, REIS D A P. Investigation on the microstructure and creep behavior of laser remelted thermal barrier coating [J]. Surface and Coatings Technology, 2019,

369: 257−264.

[20] XU Su-qin, ZHU Chao, ZHANG Yong. Effects of Laser Remelting and Oxidation on NiCrAlY/8$Y_2O_3$−$ZrO_2$ Thermal Barrier Coatings [J]. Journal of Thermal Spray Technology, 2018, 27: 412−422.

[21] DOLEKER K M, KARAOGLANL A CI, OZGURLUK Y, KOBAYASHI A. Performance of single YSZ, $Gd_2Zr_2O_7$ and double-layered YSZ/$Gd_2Zr_2O_7$ thermal barrier coatings in isothermal oxidation test conditions [J]. Vacuum, 2020, 177: 109401.

[22] AN Guo-sheng, LI Wen-sheng, FENG Li, CHENG Bo, LI Zi-yu, ZHOU Lan, WANG Zhi-ping. TGO growth behaviors and high-temperature oxidation resistance mechanism of thermal barrier coating after laser remelting [J]. The Chinese Journal of Nonferrous Metals, 2022, 32(12): 3780−3791. https://kns.cnki.net/kcms/detail/43.1238.TG.20211110.1152.002.html. (in Chinese)

[23] GOK M G, GOLLER G. Microstructural evaluation of laser remelted gadolinium zirconate thermal barrier coatings [J]. Surface and Coatings Technology, 2015, 276: 202−209.

[24] ZHAO Chang-hao, ZHAO Meng, SHAHID M, WANG Min, PAN Wei. Restrained TGO growth in YSZ/NiCrAlY thermal barrier coatings by modified laser remelting [J]. Surface and Coatings Technology, 2017, 309: 1119−1125.

[25] YAN Zheng, GUO Lei, LI Zhi-hua, YU Yang, HE Quan-jun. Effects of laser glazing on CMAS corrosion behavior of $Y_2O_3$ stabilized $ZrO_2$ thermal barrier coatings [J]. Corrosion Science, 2019, 157: 450−461.

[26] MORK M F S, BERNDT C C, DURANDET Y, BTANDT M, WANG J. Microscopic observation of laser glazed yttria-stabilized zirconia coatings [J]. Applied Surface Science, 2010, 256: 6213−6218.

[27] GUO Lei, XIN Hui, ZHANG Zhao, ZHANG Xin-mu, YE Fu-xing. Microstructure modification of $Y_2O_3$ stabilized $ZrO_2$ thermal barrier coatings by laser glazing and the effects on the hot corrosion resistance [J]. Journal of Advanced Ceramics, 2020, 9: 232−242.

[28] LIU Zheng, SHEN Zao-yu, LIU Guan-xi, HE Li-min, MU Ren-de, XU Zhen-hua. Sm-doped $Gd_2Zr_2O_7$ thermal barrier coatings: Thermal expansion coefficient, structure and failure [J]. Vacuum. 2021, 190: 110314.

[29] HAN Yu-jun, ZHU Zhi-ying, ZHANG Bao-sen, CHU Ya-jie, ZHANG Yan, FAN Jin-kai. Effects of process parameters of vacuum pre-oxidation on the microstructural evolution of CoCrAlY coating deposited by HVOF [J]. Journal of Alloys and Compounds, 2018, 735: 547−559.

[30] KARAOGLANLI A C, OZGURLUK Y, DOLEKER K M. Comparison of microstructure and oxidation behavior of CoNiCrAlY coatings produced by APS, SSAPS, D-gun, HVOF and CGDS techniques [J]. Vacuum, 2020, 180: 109609.

[31] PADTURE N P, GELL M, JORDAN E H. Thermal barrier coatings for gas-turbine engine applications [J]. Science, 2002, 296: 280−284.

[32] ZHOU Yan-chun, XIANG Hui-min, FENG Zhi-hai. Theoretical investigation on mechanical and thermal properties of a promising thermal barrier material: $Yb_3Al_5O_{12}$ [J]. Journal of Materials Science & Technology, 2014, 30: 631−638.

[33] CAI Jie, YAO Yi-ming, GAO Cheng-zuan, LU Peng, MENG Xian-kai, GUAN Qing-feng, LI Yu-xin, HAN Zhi-yong. Comparison of microstructure and oxidation behavior of NiCoCrAlYSi laser cladding coating before and after high-current pulsed electron beam modification [J]. Journal of Alloys and Compounds, 2021, 881: 160651.

[34] DOLEKER K M, OZGURLUK Y, KARAOGLANLI A C. TGO growth and kinetic study of single and double layered TBC systems [J]. Surface and Coatings Technology, 2021, 415: 127135.

[35] LU Zhe, KIM M S, MYOUNG S W, LEE J H, JUNG Y G, KIM I S, JO C Y. Thermal stability and mechanical properties of thick thermal barrier coatings with vertical type cracks [J]. Transactions of Nonferrous Metals Society of China, 2014, 24: s29−s35.

[36] CHENG Bo, WANG Yu, ZHANG Xin, AN Guo-sheng, CHU Qian-qian, ZHANG Xin-jian , HE Dong-qing , ZHAI Hai-min , LI Wen-sheng. Sintering governing the cracking behaviors of different $La_2Zr_2O_7$/YSZ ceramic layer combination TBCs at 1150 ℃ [J]. Surface and Coatings Technology, 2021, 428: 127910.

[37] ZHU Chao, LI Pu-xuan, JAVED A, LIANG Gong-ying, XIAO Ping. An investigation on the microstructure and oxidation behavior of laser remelted air plasma sprayed thermal barrier coatings [J]. Surface and Coatings Technology, 2012, 206: 3739−3746.

[38] SHI Jia-qi, ZHANG Tie-bang, SUN Bing, WANG Bing, ZHANG Xu-hu, SONG Lin. Isothermal oxidation and TGO growth behavior of NiCoCrAlY-YSZ thermal barrier coatings on a Ni-based superalloy [J]. Journal of Alloys and Compounds, 2020, 844: 156093.

[39] GHADAMI F, AGHDAM A S R, GHADAMI S. Microstructural characteristics and oxidation behavior of the modified MCrAlX coatings: A critical review [J]. Vacuum, 2021, 185: 109980.

# 激光改性 YAG/YSZ 双陶瓷热障涂层的高温氧化与 TGO 生长行为

安国升[1,2]，李文生[1,3]，王智平[2]，冯 力[1,2]，成 波[1]，周 兰[4]，李子钰[2]，张 义[2]

1. 兰州理工大学 省部共建有色金属先进加工与再利用国家重点实验室，兰州 730050；
2. 兰州理工大学 材料科学与工程学院，兰州 730050；
3. 山东科技大学 材料科学与工程学院，青岛 266590；
4. 兰州理工大学 机电工程学院，兰州 730050

**摘 要**：以 Inconel 738 合金为基体、NiCoCrAlY 为黏接层，采用大气等离子喷涂(APS)技术制备 YAG/YSZ 双陶瓷热障涂层(TBC)，并对 YAG 层表面进行激光改性，以提高 TBC 的抗高温氧化性能。通过恒温氧化实验研究喷涂态(AS)与激光改性(LM)TBC 的高温氧化及热生长氧化物(TGO)的生长行为。结果表明，AS-TBC 与 LM-TBC 的 TGO 厚度与结构呈现相似变化趋势，即厚度随氧化时间增加而增加，结构则均由单一 $Al_2O_3$ 层演变为混合氧化物层在上、$Al_2O_3$ 层在下的双层形貌。基于激光改性对氧气渗透的强烈抑制作用，LM-TBC 中混合氧化物出现的时间推迟，在氧化中后期 LM-TBC 的总体 TGO 厚度也有所减少。经过相同的氧化时间，LM-TBC 中 $Al_2O_3$ 厚度在总体 TGO 厚度中占比始终大于或等于 AS-TBC，并且 LM-TBC 的抛物线氧化速率相比 AS-TBC 下降了 18.42 %。因此，YAG/YSZ LM-TBC 呈现更优异的高温抗氧化性能与更低的 TGO 生长速率。

**关键词**：热障涂层；激光改性；双陶瓷层；氧气渗透；热生长氧化物

**(Edited by Bing YANG)**